



ELSEVIER

Available online at www.sciencedirect.com

SCIENCE @ DIRECT®

Nuclear Instruments and Methods in Physics Research B 230 (2005) 178–184

NIM B
Beam Interactions
with Materials & Atoms

www.elsevier.com/locate/nimb

Specular reflection model study of the image effect in $\text{He}^+/\text{a:Si}$ scattering at low energy

A. Hidouche ^{a,*}, A.C. Chami ^a, Y. Boudouma ^a, M. Boudjema ^{a,1}, C. Benazeth ^b

^a *Equipe de recherche "Interaction Ions-Surface", Laboratoire Sciences Nucléaires et Interactions Rayonnement-Matière, Faculté de Physique, USTHB, BP 32 El-Alia, Bab Ezzouar, Algiers, Algeria*

^b *LCAR UMR 572 UPS-CNRS 118 route de Narbonne, 31062 Toulouse Cedex, France*

Available online 22 January 2005

Abstract

Electronic polarization induced by low energy ions near solid surfaces at grazing incidence considerably modifies the collision geometry. This effect is studied by the comparison between experimental and simulated time of flight (ToF) spectra of helium ions scattered from amorphous Si for small incidence and emergence angles. In this work, we include the image effect and the external stopping power in a simulation code through the Specular Reflection Model (SRM). The image potential is computed by using the dielectric surface functions in the Random Phase Approximation (RPA), Plasmon Line Approximation (PLA) and static Thomas–Fermi approximation. With the later, it is found a better agreement with the experiment for the ionic part of the spectra.

© 2004 Elsevier B.V. All rights reserved.

1. Introduction

It has been shown in previous works [1–3] that the electronic stopping power and charge exchange probabilities can be deduced from Monte Carlo simulation compared to experimental ToF spectra obtained for low energy ions scattered from solid surfaces. Because of the different charge exchange processes occurring outside and inside the solid

(Auger neutralization or close collision charge exchange), the incident ions can hit and leave the surface as charged or neutral particle. It has been equally suggested that image potential greatly modifies the collisional geometry and provides some perturbation to the shape of the ion part of the scattered ion.

Indeed, in grazing geometry the solid exerts an attractive force on charged species owing to electronic polarization near the surface. As shown in Fig. 1, the actual incident α_s and emergence β_s angles can differ significantly from the measured (nominal) angles α_v or β_v . This effect is magnified at low energy and/or at grazing incidence (or

* Corresponding author. Fax: +213 21 247 344.

E-mail address: ahidouche@yahoo.fr (A. Hidouche).

¹ Tel.: +213 21 247 950; fax: +213 21 247 344.

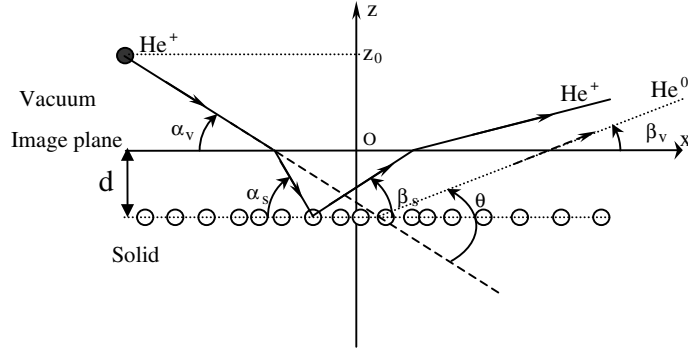


Fig. 1. Image potential effect on the charged in the vicinity of a solid surface. The incident, emergent and scattering angles are defined (see text).

emergence). The actual and measured angles are related by the equation:

$$\tan \begin{pmatrix} \alpha_s \\ \beta_s \end{pmatrix} = \tan \begin{pmatrix} \alpha_v \\ \beta_v \end{pmatrix} \left(1 + \frac{V_{\text{im}}}{E \sin^2 \begin{pmatrix} \alpha_v \\ \beta_v \end{pmatrix}} \right)^{1/2}, \quad (1)$$

where E is the incident energy of the incoming ion, V_{im} represents the total image potential. The image plane (at $z = 0$) defines the “effective surface position” [4] so that the asymptotic potential felt by a positively singly charged ion far from the surface tends to the classical image potential [5]: $V_{\text{im}}^{\text{class}}(z) = -\frac{1}{4z}$. (We use atomic units throughout this work.)

2. The specular reflection model

The image potential, and more generally, the polarization of a semi-infinite solid due to a point charge perturbation requires the knowledge of the self-consistent dielectric function. In the Specular Reflection Model (SRM) proposed by Ritchie and Marusak [6], the solid is described as a jellium ended by an abrupt surface. The electrons participating to the response are specularly reflected at the surface so that the electronic density vanishes outside the solid. In this model, the response of the semi-infinite medium like the induced potential can be obtained through the surface dielectric function $\varepsilon_s(\mathbf{Q}, \omega, z)$ given by [7]

$$\varepsilon_s(\mathbf{Q}, \omega, z) = \frac{Q}{\pi} \int_{-\infty}^{+\infty} dk_z \frac{e^{ik_z z}}{(k_z^2 + Q^2) \varepsilon(\mathbf{k}, \omega)}, \quad (2)$$

where $k^2 = k_z^2 + Q^2$, $\varepsilon(\mathbf{k}, \omega)$ is the bulk dielectric function for an infinite and isotropic solid, (\mathbf{k}, ω) represent respectively the wave vector and the frequency of a perturbation at which the electronic response is evaluated, and z is the coordinate normal to the solid surface.

In the limit of a point charge projectile with charge Z_1 and with velocity $\mathbf{v} = (v_{\perp}, v_{\parallel})$ at a distance z_0 from the surface (the origin is taken at the image plane), the induced potential inside and outside the solid can be computed. For grazing incidence and emergence of the projectile, $\mathbf{v} \approx (0, v_{\parallel})$ the induced potential ϕ_{ind} at the projectile, and the image potential $V_{\text{im}}(z_0)$ are given by

$$V_{\text{im}}(z_0) = \frac{Z_1}{2} \phi_{\text{ind}}(x = vt, y = 0, z = z_0) = \begin{cases} \frac{Z_1^2}{4\pi} \int_{\mathbf{Q}} \frac{1}{Q} \left[\varepsilon_s^{2z_0} + \varepsilon_s^0 - \frac{2(\varepsilon_s^{z_0})^2}{\varepsilon_s^0 + 1} - 1 \right] d\mathbf{Q}, & z_0 < 0, \\ \frac{Z_1^2}{4\pi} \int_{\mathbf{Q}} \frac{e^{-2Qz_0}}{Q} \left(\frac{\varepsilon_s^0 - 1}{\varepsilon_s^0 + 1} \right) d\mathbf{Q}, & z_0 > 0, \end{cases} \quad (3)$$

with $\varepsilon_s^z = \varepsilon_s(\mathbf{Q}, \mathbf{Q} \cdot \mathbf{v}_{\parallel}, z)$. In the static limit ($v \rightarrow 0$), and far from the solid surface, this relation tends toward the classic expression: $V_{\text{im}}(z_0) \approx -\frac{Z_1^2}{4z_0}$.

The total image potential V_{im} is defined by the value of the image potential deep inside the bulk ($V_{\text{im}} = V_{\text{im}}(-\infty)$).

Three main approximations, briefly recalled below, are generally used for the calculation of the bulk dielectric function:

(i) *Random phase approximation* [8]. For a totally degenerated electron gas, the bulk dielectric function is

$$\varepsilon(\mathbf{k}, \omega) = 1 + \frac{2}{k^2} \frac{\omega_0^2}{(2\pi)^3 n} \times \int_{|\mathbf{q}| \leq k_{\text{F}}} \left(\frac{1}{k^2 + 2\mathbf{k} \cdot \mathbf{q} - 2\frac{m}{\hbar}(\omega + i\delta)} + \frac{1}{k^2 - 2\mathbf{k} \cdot \mathbf{q} + 2\frac{m}{\hbar}(\omega + i\delta)} \right) d\mathbf{q}, \quad (4)$$

where ω_0 is the plasmon frequency of the electronic gas, n is its density related to a mean electron radius $r_s = (3/4\pi n)^{1/3}$ and \mathbf{q} represents the electron wave vector. δ is an infinitesimal positive quantity characteristic of oscillation damping. It has been established by Garcia de Abajo and Echenique [9] that the induced potential inside and outside the solid depends weakly on the projectile velocity, between 0 and 0.2 a.u. So, the static approximation can be used in the present case of 4 keV He^+ projectile ($v = 0.2$ a.u.). An expression of ε_s^z for low energy ions has been previously established in this way [10].

(ii) *Plasmon line approximation* [11].

$$\varepsilon(\mathbf{k}, \omega) = 1 + \frac{\omega_0^2}{\beta^2 k^2 + \lambda \frac{k^4}{4} - \omega(\omega + i\delta) - \omega_g^2}, \quad (5)$$

$$\beta = \sqrt{3/5} \frac{1.919}{r_s},$$

ω_g is the energy gap of the solid and λ is an adjustable parameter determined from Kato's cusp condition [12].

(iii) *Static Thomas–Fermi approximation* [13].

$$\varepsilon(\mathbf{k}) = 1 + \frac{k_{\text{TF}}^2}{k^2}, \quad k_{\text{TF}} = 1.56/\sqrt{r_s} \text{ (a.u.)}. \quad (6)$$

This last approximation is only valid for very slow projectiles typically when $v \ll 1$ a.u.

3. Results and discussion

3.1. Image effect

In Fig. 2 the evolution of the image potential versus the distance at the image plane is shown for the PLA approximation for the electronic density suitable for Si ($r_s = 1.97$). The classical image potential is also reported. It can be seen from these results that the image force is maximal in the vicinity of the image plane. So, the ionic trajectory is strongly deviated around the image plane as schematized in Fig. 1. In Eq. (5), the electronic gap ω_g of the Si explicitly appears. However, the obtained image potentials with and without the gap, lead to approximately the same result. This result tends to valid the approximation of free electron gas used for the other models. In Table 1, the different values of the total image potential are given for the different bulk dielectric functions used. A great dispersion in the values is obtained, and the dynamical values remain smaller than the static Thomas–Fermi value used by Kato et al. [14]. The comparison with the experimental results is required to discriminate between the different approximations and also to test the validity of the dielectric treatment of the electronic response

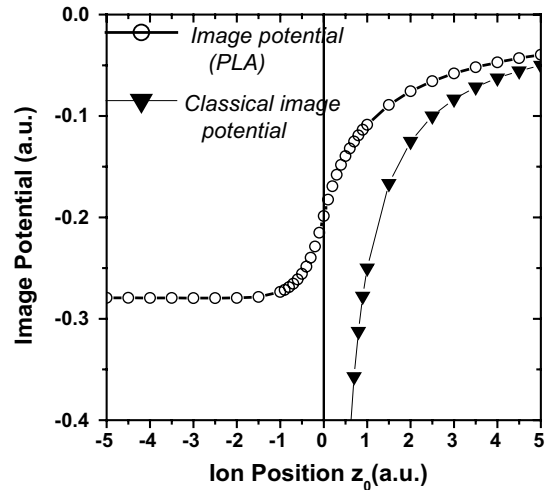


Fig. 2. Image potential versus normal distance between the projectile and the image plane for density suitable for Si ($r_s = 1.97$).

Table 1

Total image potentials obtained in various approximations for the bulk dielectric functions $\epsilon(\mathbf{k}, \omega)$

Approximation	V_{im} (eV)
RPA	10.1
PLA ($\lambda = 1$)	7.6
PLA	5.5
TF [14]	15.0

of the solid. To make connection to the actual incident and emergence angle experienced by a positively charged projectile, we represent in Fig. 3, the relation between α_s and α_v (resp. β_s and β_v) for the different approximations used. It can be seen that, in the present experimental conditions, the difference between α_s and α_v (resp. β_s and β_v) vanishes for nominal emergence angles greater than 7° i.e. for scattering angles greater than 13° . In these conditions, the image effect cannot influence the geometry of the collisions.

3.2. Experiments

The experimental setup has been previously described in detail [1–3,15]. Briefly, He^+ beam of 4 keV is directed toward an amorphized Si target. The incident angle is 6° , the ToF arrangement is able to detect the scattered projectiles from 0° up to 165° . The ultra high vacuum prevents surface

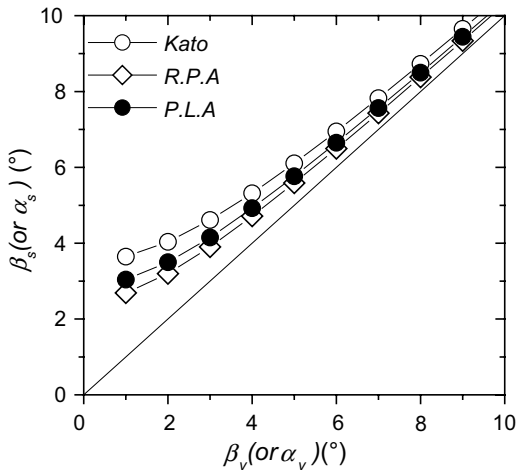


Fig. 3. Variation of the actual α_s (resp β_s) versus nominal α_v (resp β_v) angles.

contamination after sputter surface cleaning by a Ne^+ beam. This beam is also used to amorphize the Si near surface target. A post-acceleration in the ToF arrangement discriminates between the various charge states of the detected species. Typical spectra obtained in the angular scan are reported in Fig. 4. Together with the experimental spectra, are shown the corresponding results of the simulated spectra at each scattering angle. On Fig. 5, angular scan spectra are shown for very low emergence angles.

3.3. Simulations

Monte Carlo simulations of multiple scattering collisions are performed using a code previously described [1–3]. Several parameters as charge exchange probabilities and friction coefficient γ of the electronic stopping power are extracted from comparison between experimental and simulated ToF spectra at various scattering angles. The two processes of charge exchange between He and Si are taken into account. Let ‘ a ’ be the characteristic length of the electronic density decay beyond the image plane. The Auger neutralization is found to be characterized by a parameter $(a + d)/\lambda_{\text{Auger}} = 0.083$ a.u. quite close to the previous result 0.072 of Arezki et al. [1]. λ_{Auger} is the ion mean free path for Auger neutralization. The close collision ionization or neutralization probability (assumed to be equal) is $P_I = P_N = 0.41$, confirming somewhat the value of 0.34 obtained for Si(100)-(2 × 1) surface interacting with 5 keV He^+ ions [16]. A good fit is obtained for the all spectra at scattering angles greater than about 13° . This agreement is valid for both neutral part and for ionic part (Fig. 4). However, a clear discrepancy appears for smaller angles (Fig. 5).

On the other hand, assuming the same value of the electronic friction coefficient γ for both He^+ and He^0 , the best fit of the ToF spectra corresponds to an electronic friction coefficient $\gamma = 0.322$ a.u. at this projectile velocity. This value is comparable to the Density Functional evaluation $\gamma = 0.27$ a.u. computed elsewhere, taken the Si band gap into account [2].

At small scattering angles, the actual emergence angle β_s of a charged He^+ is different from the

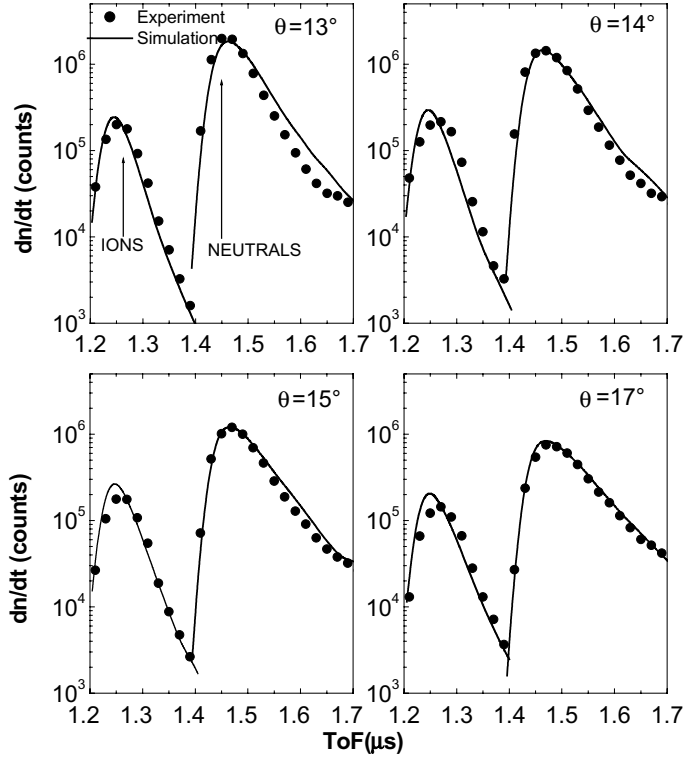


Fig. 4. Comparison between experimental (●) and simulated (—) ToF spectra for scattering angles greater than 13° . The incident angle is 6° and the He^+ incident energy is 4 keV.

nominal one β_v . So for the ion, at a given scattering angle, β_v is replaced in the simulation by β_s , while it is still used for the neutral particle. This effect is significant in particular, for scattering angles lower than 13° .

Taking into account such an effect greatly enhances the agreement between the simulated and the experimental ion part of the spectra as can be observed from Fig. 5. The best agreement is obtained for the Kato et al. [14] value of the total image potential i.e. $V_{\text{im}} = 15$ eV. This value is consistent with that obtained for the He^+/Ni system [3].

3.4. External stopping power

Owing to the electron polarization inside the solid due to the presence of a charged particle near the surface, the projectile is subjected to a friction force parallel to the surface. This force or stopping

power is directly related to the induced potential and can be computed in the frame of the SRM [10]:

$$S_c(z_0, v) = -Z_1 \frac{\partial \phi_{\text{ind}}}{\partial x}(x = vt, y = 0, z = z_0). \quad (7)$$

The total energy loss in the exit phase of the charged ion is then:

$$\Delta E_s = \int_0^\infty \frac{S_c(z_0, v)}{\sin(\beta_v)} \cdot dz_0. \quad (8)$$

In this relation, it is considered that the external energy loss is mainly produced from the image plane in the exit phase and with an emergence angle β_v . This approximation is related to the discussion in Section 3.1. The total energy loss value is noticeable for low values of the emergence angle. It is found $\Delta E_s(\beta_v = 1^\circ) = \Delta E_s(\theta = 7^\circ) = 123$ eV and $\Delta E_s(\beta_v = 2^\circ) = \Delta E_s(\theta = 8^\circ) = 61$ eV. At higher values of the scattering angle θ , ΔE_s cannot be

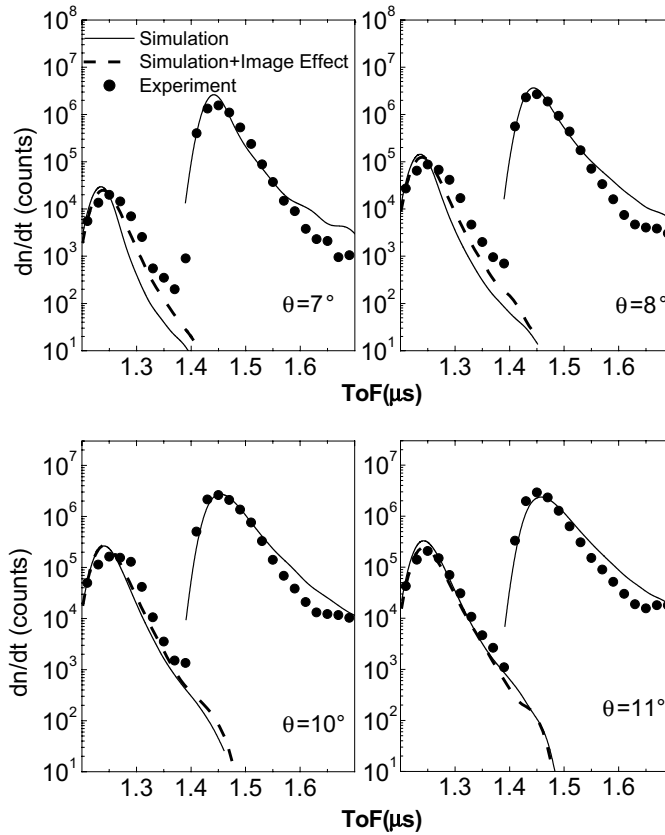


Fig. 5. Same as Fig. 4 but for low scattering angles (lower than 13°). The dashed lines are related to the image potential correction.

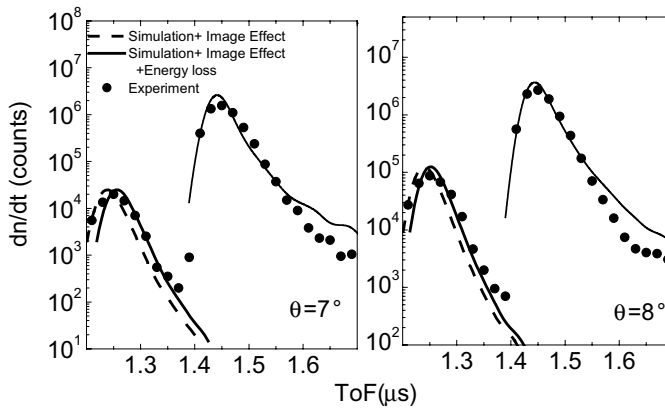


Fig. 6. Experimental and simulated spectra for scattering angles $\theta = 7^\circ$ and $\theta = 8^\circ$. The dashed lines are related to the image potential correction, the solid lines correspond to image potential and external stopping power corrections.

estimated owing to the energy resolution of the ToF arrangement which is about 100 eV at this en-

ergy. It should be noticed that in spite of the fact that the ionic fraction impinging the solid surface

is quite important, the external energy loss should be very low owing to the relative important incident angle ($\alpha_v = 6^\circ$). In Fig. 6 the effect of the external energy loss in the exit phase on the spectra simulation is represented for $\theta = 7^\circ$ and 8° . The agreement with the experimental spectra is enhanced.

4. Conclusion

In this work, ToF spectra of low energy He^+ ions ($E_\alpha = 4 \text{ keV}$) scattered at various angles by an amorphized Si surface are simulated through a Monte Carlo code. A good agreement is obtained for both neutral and charged scattered projectiles at higher emergence angles. However, for grazing emergence angles, the agreement is not so good particularly for charged ions. The difference is treated by introducing two phenomena that can modify collisional geometry at low emergence angles. The first one is related to the image potential acting on the charged projectile resulting in a difference between the emergence angle at the solid surface and the detection angle. The second is due to inelastic energy loss in the vicinity of the surface in grazing geometry. Quantitative evaluation of these effects, are computed in the linear electronic response framework and the SRM is used to reproduce the surface limit of the solid. The obtained image potential is shown to depend strongly on the dielectric function chosen for the solid. With a total image potential close to 15 eV, it is found that the agreement is greatly enhanced for the ionic part of the ToF spectra.

In order to get more insight in the problem of image potential, it would be interesting to go beyond the linear response theory. On the experimental side, well defined crystalline surface at very low projectile energy would give maximum

sensitivity to image effect. Analysis of the ionic part of the scattered energy distribution would be of great interest.

References

- [1] B. Arezki, Y. Boudouma, P. Benoit-Cattin, A.C. Chami, C. Benazeth, K. Khalal, M. Boudjema, *J. Phys.: Condens. Matter* 10 (1998) 741.
- [2] M. Boudjema, N. D'Bichi, Y. Boudouma, A.C. Chami, B. Arezki, K. Khalal, C. Benazeth, P. Benoit-Cattin, *Nucl. Instr. and Meth. B* 164–165 (2000) 588.
- [3] R. Zemih, M. Boudjema, C. Benazeth, Y. Boudouma, A.C. Chami, *Nucl. Instr. and Meth. B* 193 (2002) 401.
- [4] P.J. Jennings, R.O. Jones, H. Weinert, *Phys. Rev. B* 37 (1988) 6133;
S. Ossicini, C.M. Bertoni, *Europhys Lett.* 1 (1986) 661.
- [5] J.D. Jackson, *Classical Electrodynamics*, second ed., Wiley, New York, 1974.
- [6] R.H. Ritchie, A.L. Marusak, *Surf. Sci.* 4 (1966) 234.
- [7] J. Heinrichs, *Phys. Rev. B* 8 (1973) 1346;
P.M. Echenique, R.H. Ritchie, N. Barberan, J. Inkson, *Phys. Rev. B* 23 (1981) 6486.
- [8] J. Lindhard, A. Winther, *Mat. Fys. Medd. Dan. Vid. Selk.* 34 (1964) 1.
- [9] F.J. Garcia de Abajo, P.M. Echenique, *Phys. Rev. B* 48 (1993) 13399.
- [10] Y.-N. Wang, W.-K. Liu, *Phys. Rev. A* 54 (1996) 636.
- [11] R.H. Ritchie, W. Brandt, P.M. Echenique, *Phys. Rev. B* 14 (1976) 4808.
- [12] I. Nagy, A. Arnau, P.M. Echenique, *Phys. Rev. B* 48 (1993) 5650;
I. Nagy, B. Apagyi, K. Ladanyi, in: A. Gras-Marti, H.M. Urbassek, N.R. Arista, F. Flores (Eds.), *Interaction of Charged Particles with Solids and Surfaces*, NATO ASI Series, Vol. B271, Plenum, New York, 1990, p. 395.
- [13] J.W. Gadzuk, *Surf. Sci.* 23 (1970) 58.
- [14] M. Kato, R.S. Williams, M. Aono, *Nucl. Instr. and Meth. B* 33 (1988) 462.
- [15] C. Benazeth, P. Benoit-Cattin, P. Cafarelli, P. Reynes, J.P. Ziesel, N. Benazeth, *Nucl. Instr. and Meth. B* 94 (1994) 581.
- [16] I. Vaquilla, I.L. Bolotin, T. Ito, B.N. Makarenko, J.W. Rabalais, *Surf. Sci.* 496 (2002) 187.